

Anisotropic Dependence of Superconductivity on Uniaxial Pressure in CeIrIn₅

O. M. Dix, A. G. Swartz, and R. J. Zieve

Department of Physics, University of California Davis, Davis, California 95616, USA

J. Cooley

Material Science and Technology Division, Los Alamos National Laboratory, Los Alamos, New Mexico 87545, USA

T. R. Sayles* and M. B. Maple

Department of Physics, University of California San Diego, San Diego, California 92093, USA

(Received 23 October 2008; published 11 May 2009)

We measure the effect of uniaxial pressure on the superconducting transition temperature T_c in CeIrIn₅. We find a linear change in T_c with both a -axis and c -axis pressure, with slopes of 56 and -66 mK/kbar, respectively. By comparing results from doping studies and different types of pressure measurements, we separate the influences of hybridization and dimensionality on T_c . We find the true geometric influence, for constant hybridization, is $\partial T_c / \partial(c/a) = 44$ K.

DOI: 10.1103/PhysRevLett.102.197001

PACS numbers: 74.70.Tx, 74.25.Bt, 74.62.Fj

The low-temperature phases of heavy fermion materials have attracted much attention in recent years. They exhibit a range of correlated phases, including several types of magnetism. Superconducting regimes emerge near zero-temperature magnetic phase transitions. Non-Fermi liquid behavior also appears near these quantum critical points, and can persist to significant temperatures. Tuning through alloying, pressure, or applied field allows exploration of the exact balance among the phases.

One of the most-studied heavy fermions recently has been CeMIn₅ ($M = \text{Ir, Rh, Co}$). The proximity of these Ce-based 115 compounds to an antiferromagnetic quantum critical point leads to a rich phase diagram [1]. CeRhIn₅ at ambient pressure has a superconducting transition near 0.1 K, deep within an antiferromagnetic phase [2]. Hydrostatic pressure destroys the magnetism and raises T_c to a maximum of 2.1 K at 16 kbar [3,4]. On the other hand, CeIrIn₅ and CeCoIn₅ superconduct at ambient pressure [5,6], with several similarities to the high-temperature cuprate superconductors. The 115 materials have a tetragonal, HoCoGa₅ crystal structure which can be viewed as alternating layers of CeIn₃ and MIn₂ stacked along the (0 0 1) direction [3,5,6], reminiscent of the copper-oxygen planes in the cuprates. Power-law temperature dependences in heat capacity, thermal conductivity and spin-lattice relaxation rate in the superconducting state suggest d -wave symmetry of the superconducting order parameter [7]. Furthermore, emergence of superconductivity near T_N and coexistence of homogeneous antiferromagnetism and superconductivity provide evidence that magnetic fluctuations mediate Cooper-pairing in these systems [8–10].

One major influence on the superconducting transition temperature is the hybridization between the Ce f -electrons and In p electrons [11–13], which controls the spin-fluctuation temperature, T_{sf} . T_{sf} is proportional to T_c and roughly inversely proportional to γ , the

Sommerfeld coefficient of the normal-phase specific heat. Smaller γ 's in the isostructural PuMGa₅ compounds ($M = \text{Rh, Co}$) partially account for their much higher superconducting transition temperatures. However, even within the CeMIn₅ series, γ alone cannot describe all the variation in T_c ; for example, while γ changes by just over a factor of 2 between $M = \text{Ir}$ and $M = \text{Co}$, T_c changes by nearly a factor of 6. Thus hybridization cannot be the sole influence on T_c .

Mean-field theoretical models of magnetically mediated superconductivity indicate a strong dependence of T_c on dimensionality [14–16]. Measurements on CeM_{1-x}M'_xIn₅ show a linear relationship between T_c and the ratio of the tetragonal lattice constants c/a [8]. Interestingly, for the Pu-based 115 materials T_c is also linear in c/a , with the same relative change in T_c with dimensionality, $\frac{1}{T_c} \frac{dT_c}{d(c/a)}$ [11]. The agreement in slopes makes sense if the difference in hybridization sets the overall temperature scale for each family but dimensionality governs the behavior within each family. Another way to control dimensionality and hybridization is by applying pressure. Under hydrostatic pressure, c/a is not even monotonic for CeRhIn₅ and CeCoIn₅, and T_c is not linear in c/a . However, all the CeMIn₅ compounds have similar hybridization at the pressure P_{max} which maximizes the T_c . Considering T_c and c/a at P_{max} , where the effects of hybridization differences are reduced, does give a linear relationship [12,17]. Kumar *et al.* argue that hydrostatic pressure mainly alters the hybridization. The similar hybridizations at P_{max} suggest that hybridization determines the pressure P_{max} while dimensionality governs the value of T_c at P_{max} [12].

Uniaxial pressure is a natural technique for further exploring the effects of dimensionality, since the c/a ratio of an individual sample can be increased or decreased depending on the pressure axis. Uniaxial pressure leads to fairly small changes in hybridization, since lattice con-

stants decrease along the direction of applied force but increase in the perpendicular directions. On the other hand, the effects on c/a are much larger than for a similar hydrostatic pressure. To date, the effects of uniaxial pressure on the 115 materials have not been measured directly, although thermal expansion measurements combined with Ehrenfest relations predict the change in T_c with uniaxial pressure in the zero-pressure limit [18]. Here we explore the dependence of T_c on pressure and hence on c/a , and combine our results with those on hydrostatic pressure and alloying to extract the dependence of T_c on dimensionality.

Samples were grown in alumina crucibles from a molten metal flux containing stoichiometric amounts of Ce and Ir, and excess indium. We confirmed through transmission Laue x-ray diffraction that the lattice constants of our samples matched those reported elsewhere [19].

Our uniaxial pressure apparatus, shown in Fig. 1, is a helium-activated bellows mounted on a dilution refrigerator [20], and permits changes in pressure without thermally cycling the sample. We monitor the pressure through a piezoelectric crystal in the pressure column. The maximum achievable pressure depends on the size of the sample, but is typically about 10 kbar. We measure the superconducting transition with adiabatic heat capacity. Superconducting NbTi spacers between the sample and the pressure cell serve as the thermal link.

As can be seen from Fig. 1, the sample is unconstrained in directions perpendicular to applied pressure. To apply pressure along a specific axis, we first orient our sample using Laue x-ray diffraction. We then polish the sample according to the desired orientation. We preserve as much bulk as possible during the polishing, since the observed time constant for thermal decay is proportional to the sample's mass. Our largest samples for pressure along the c and a axes were approximately 30 and 80 mg, respectively.

Figure 2 shows representative heat capacity data. Pressure applied along the c axis shifts the transition to lower temperature, while a -axis pressure has the opposite effect. The data are scaled, with a single scaling constant used for each sample, regardless of pressure. The average C/T over all pressures at 800 mK is set to 700 mJ/mol K².

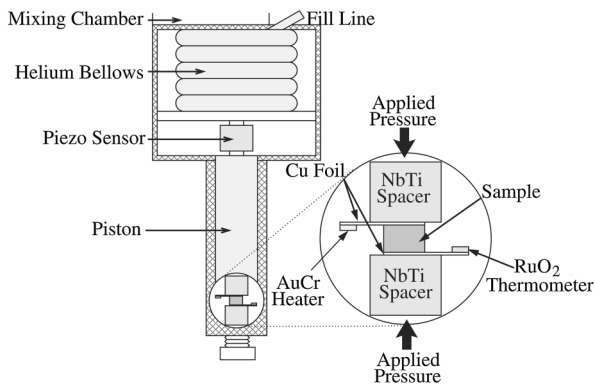


FIG. 1. Helium bellows setup for measuring heat capacity under uniaxial pressure.

For a -axis pressure, we fit a function $\gamma_s + a_1 T^n + a_2 T^{-3}$ to the heat capacity in the superconducting phase [5]. The form fits well at all pressures, with the exponent n always close to 1, as expected for line nodes in the energy gap. For c -axis pressure, the reduced T_c leaves too small a temperature range for reliable fits. If we fix $n = 1$ and refit the data, we find a slight decrease in both γ_s and a_1 with pressure, as opposed to the sharp change in γ_s observed with uniaxial [20] and hydrostatic [21,22] pressure in other heavy fermion superconductors.

We define T_c as the temperature where C/T equals the average of its maximum value in the superconducting region and its value in the normal phase at the onset of the transition. We also model the transition as an abrupt discontinuity with the restriction that the normal-phase entropy is the same as for the actual data. The two methods give consistent values of T_c . However, under c -axis pressure T_c decreases until eventually there is not enough data in the superconducting region to extrapolate the value of C/T in an equal-entropy calculation. For consistency between c - and a -axis pressure, all values we report here use the average- C/T method for T_c in both pressure directions. The transition temperatures for different pressures, obtained using this average C/T method, are shown in Fig. 3. In our pressure range, the change in T_c is linear. It equals 56 mK/kbar for a -axis pressure, -66 mK/kbar for c -axis pressure. These values agree fairly well with those derived for the zero-pressure limit from thermal expansion data: 54 and -89 mK/kbar, respectively [18]. For the tetragonal crystal structure, we can also compare our results to the effect of hydrostatic pressure through $\partial T_c / \partial p_V = 2\partial T_c / \partial p_a + \partial T_c / \partial p_c$. Our data yield a value of $\partial T_c / \partial p_V = 46$ mK/kbar, somewhat larger than the 25 mK/kbar obtained through direct hydrostatic pressure measurements [23].

We also comment on the normal state heat capacity. We find no significant change with a -axis pressure but an

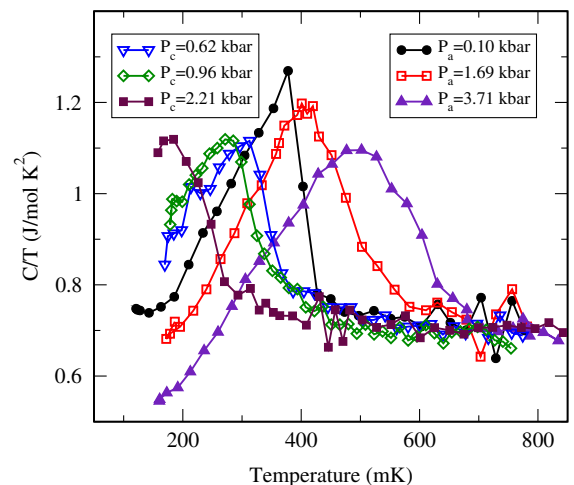


FIG. 2 (color online). Heat capacity at various pressures. The data have been scaled by the normal-phase heat capacity; see text.

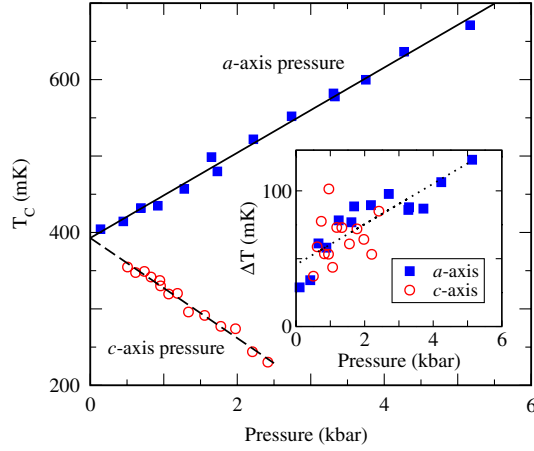


FIG. 3 (color online). Transition temperature as a function of uniaxial pressure. T_c was determined using the temperature corresponding to the average of the C/T values at the peak and onset of the transition. Lines are linear fits, with slope 56 and -66 mK/kbar. Inset: 20%–80% transition width vs pressure. The dotted line is a guide to the eye.

increase 0.03 ± 0.01 J/kbar mol K^2 with c -axis pressure. Previous hydrostatic pressure measurements [23] found a decrease of -0.02 J/kbar mol K^2 . Although the sign differences here and in $\delta T_c / \delta P$ may be related, the magnitudes of the heat capacity changes do not correspond to the overall Ce-In hybridization for the different types of pressure. Instead they suggest that hybridization in certain directions affects the heat capacity more than in others. The superconducting jump averages $\Delta C / \gamma T_c = 0.73 \pm 0.05$ J/mol K^2 and has no apparent trend with pressure, consistent with previous experiments [5,19,23].

We take as the width of the transition the span between the temperatures corresponding to 20% and 80% of the C/T range during the transition, as shown in the inset of Fig. 3. Under pressure the transition becomes broader and more rounded. Although an inhomogeneous pressure distribution across the face of the sample or a variation in the cross-sectional area over the height of the sample would broaden the transition, reasonable values for these effects would produce less than 15% of the observed broadening.

We apply a small pressure during cooldown to keep the sample in place. This initial pressure differs for each cooldown but is typically on the order of 0.3 kbar. To determine the initial pressure, we extrapolate T_c versus p to where the transition temperature reaches that measured on samples outside of the pressure cell. The pressure labels for the curves in Fig. 2 are adjusted for the initial pressure, so that the values listed are the correct pressures.

Figure 4 redisplayes the data of Fig. 3 to T_c as a function of c/a . We use room temperature lattice constants [19] and the elastic constants of CeRhIn₅ [17] to compute c/a at different pressures [19]. We assume that the CeIrIn₅ elastic constants are similar [18]. Also, at our low to moderate pressures, the stress-strain relations are still linear.

Just as for measurements across the CeMn₅ family, we find that T_c increases with increasing c/a . The dotted line of Fig. 4 is at the ambient-pressure value for c/a . Applying c -axis pressure decreases c while increasing a through the Poisson ratio, so the data from c -axis pressures appear to the left of the dotted line. On the other hand, a -axis pressure decreases the a lattice constant along the pressure direction and increases c , but also increases the a -axis lattice constant perpendicular to the pressure direction. Since the largest change in lattice constant is along the pressure direction, the overall effect is an increase in c/a , and the a -axis data appear to the right of the dotted line. However, for a -axis pressure the ratio c/a is not a single well-defined quantity. The value of a is minimum in the direction parallel to the applied pressure and maximum perpendicular to the pressure. Both of these extreme values are used to calculate c/a , with the results plotted in Fig. 4. The remaining data set in Fig. 4 uses the geometric mean of the maximum and minimum a values, which is the natural way to compare in-plane areas with the perpendicular lattice constant. As seen in Fig. 4, using the mean value gives a kink in $dT_c/d(c/a)$ at the crossover from c -axis to a -axis pressure. The larger slope of the a -axis data may indicate the influence of hybridization. Since the hybridization depends on the spacing between atoms, it increases for both directions of uniaxial pressure. However, the increase is small because the decrease in atomic spacing along the direction of the applied pressure is partly compensated by increased spacings in the perpendicular directions.

By considering several different methods of shifting T_c , we can separate the true influence of geometry on the

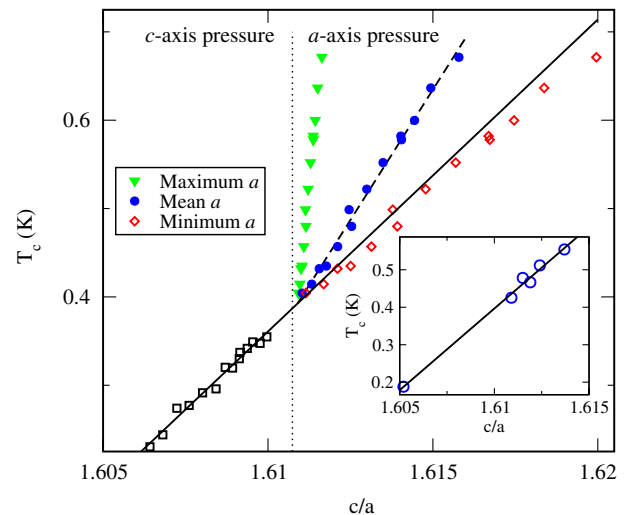


FIG. 4 (color online). T_c vs c/a . For a -axis pressure, we calculate c/a using the minimum, geometric mean, and maximum a values; see text for details. The solid line is a least-squares fit to the c -axis data, with slope 35 K. The dashed line is a least-squares fit to the a -axis data using the mean values for a . Inset: putative T_c vs c/a from substitution and pressure data, with hybridization potential V_{pf} equal for all points.

TABLE I. Values used in adjusting for effect of hybridization changes on T_c . Zero-pressure structural parameters from [19,24]; hydrostatic pressure data are from [12]. See discussion in text.

| | T_c (K) | c/a | V_{pf} | $\Delta V_{pf}(\%)$ | T_c (K) at $\Delta V_{pf} = 0.2\%$ | c/a at $\Delta V_{pf} = 0.2\%$ |
|--|-----------|--------|----------|---------------------|---|-------------------------------------|
| CeIrIn ₅ ($P = 0$) | 0.40 | 1.6109 | 2.0240 | ... | ... | ... |
| CeIrIn ₅ (29 kbar) | 1.05 | 1.6099 | 2.1277 | 5.1 | 0.4254 | 1.6109 |
| CeCoIn ₅ ($P = 0$) | 2.30 | 1.6368 | 2.0930 | 3.4 | 0.5116 | 1.6124 |
| CeCoIn ₅ (14 kbar) | 2.60 | 1.6435 | 2.1578 | 6.6 | 0.4666 | 1.6119 |
| CeRhIn ₅ (24 kbar) | 2.50 | 1.6270 | 2.1326 | 5.4 | 0.4783 | 1.6115 |
| CeIrIn ₅ (5.17 kbar, a -axis) | 0.67 | 1.6158 | 2.0312 | 0.35 | 0.5543 | 1.6137 |
| CeIrIn ₅ (2.42 kbar, c -axis) | 0.23 | 1.6063 | 2.0273 | 0.16 | 0.1880 | 1.6052 |

transition temperature from the effect of hybridization. To do this, in Table I we consider the effects of hydrostatic pressure, chemical substitution, and our a -axis and c -axis pressure measurements. We use Harrison's calculation [25]

of V_{pf} in a tight binding approximation, $\eta_{pf} \frac{\hbar^2}{m} \sqrt{\frac{r_p r_f^5}{d^5}}$. Here $\eta_{pf} = 10\sqrt{21}/\pi$ is a dimensionless constant, m is the electron mass, and $r_f = 0.445 \text{ \AA}$ and $r_p = 19.1 \text{ \AA}$ are wave function radii [12,26]. For r_p we extrapolate values from [26], p. 644. For hydrostatic pressure data, we take the percentage changes in V_{pf} and c/a from Table II and Fig. 2 of [12].

Each experiment in Table I—substitution, applied pressure, or a combination of the two—increases V_{pf} over its value in CeIrIn₅ at ambient pressure, with a percent change given by ΔV_{pf} . For each type of measurement we simultaneously scale the changes in T_c , c/a , and V_{pf} by a single factor to reach $\Delta V_{pf} = 0.2\%$. Our scaled values show how T_c would vary as a function of c/a with V_{pf} held constant. The results from the final two columns of Table I also appear in the inset of Fig. 4. The solid line is a best fit to all six points, with slope 44 K. Significantly, the slope remains 44 K if the fit omits the c -axis pressure data, which has particularly small hybridization change and lies far from the other points.

The broken symmetry perpendicular to the c axis when pressure is applied along the a axis has little effect on the superconductivity, judging from the linearity of the fit in the Fig. 4 inset. We note that using the minimum value of the lattice constant a preserves the linearity of T_c vs c/a . Although probably coincidental, this may indicate how the destruction of tetragonal symmetry affects the superconductivity.

Our measurements show that up to a few kbar T_c changes linearly with uniaxial pressure, at 56 mK/kbar for a -axis pressure and -66 mK/kbar for c -axis pressure. This confirms the important role of c/a in controlling the onset of superconductivity. Changes in fp hybridization between the Ce and neighboring In atoms also have a large effect. By comparing several techniques that alter the dimensionality and the hybridization to different degrees, we control for hybridization changes and find a pure geometric influence of $\partial T_c / \partial (c/a) = 44$ K.

We thank S. Johnson for useful discussions and J. Ma for helping to polish the samples. We acknowledge support from NSF under DMR-0454869 and DMR-0802478.

*Present address: Quantum Design, 6325 Lusk Boulevard, San Diego, CA 92121, USA.

- [1] L. D. Pham, T. Park, S. Maquilon, J. D. Thompson, and Z. Fisk, Phys. Rev. Lett. **97**, 056404 (2006).
- [2] J. Paglione *et al.*, Phys. Rev. B **77**, 100505(R) (2008).
- [3] H. Hegger *et al.*, Phys. Rev. Lett. **84**, 4986 (2000).
- [4] J. D. Thompson *et al.*, J. Magn. Magn. Mater. **226**, 5 (2001).
- [5] C. Petrovic *et al.*, Europhys. Lett. **53**, 354 (2001).
- [6] C. Petrovic *et al.*, J. Phys. Condens. Matter **13**, L337 (2001).
- [7] J. D. Thompson *et al.*, Physica (Amsterdam) **329–333B**, 446 (2003).
- [8] P. G. Pagliuso *et al.*, Physica (Amsterdam) **312–313B**, 129 (2002).
- [9] T. Mito *et al.*, Phys. Rev. Lett. **90**, 077004 (2003).
- [10] S. Kawasaki *et al.*, Phys. Rev. Lett. **96**, 147001 (2006).
- [11] J. D. Thompson, J. L. Sarrao, and F. Wastin, Chin. J. Phys. (Taipei) **43**, 499 (2005).
- [12] R. S. Kumar, A. L. Cornelius, and J. L. Sarrao, Phys. Rev. B **70**, 214526 (2004).
- [13] S. Fujimori *et al.*, Phys. Rev. B **73**, 224517 (2006).
- [14] N. D. Mathur *et al.*, Nature (London) **394**, 39 (1998).
- [15] P. Monthoux and G. G. Lonzarich, Phys. Rev. B **63**, 054529 (2001).
- [16] P. Monthoux and G. G. Lonzarich, Phys. Rev. B **66**, 224504 (2002).
- [17] R. S. Kumar *et al.*, Phys. Rev. B **69**, 014515 (2004).
- [18] N. Oeschler *et al.*, Phys. Rev. Lett. **91**, 076402 (2003).
- [19] Y. Haga *et al.*, Phys. Rev. B **63**, 060503(R) (2001).
- [20] R. J. Zieve, R. Duke, and J. L. Smith, Phys. Rev. B **69**, 144503 (2004).
- [21] R. Caspary *et al.*, Phys. Rev. Lett. **71**, 2146 (1993).
- [22] R. A. Fisher *et al.*, J. Supercond. **15**, 433 (2002).
- [23] R. Borth *et al.*, Physica (Amsterdam) **312–313B**, 136 (2002).
- [24] T. Maehira, T. Hotta, K. Ueda, and A. Hasegawa, J. Phys. Soc. Jpn. **72**, 854 (2003).
- [25] J. M. Wills and W. A. Harrison, Phys. Rev. B **28**, 4363 (1983).
- [26] W. A. Harrison, *Elementary Electronic Structure* (World Scientific Publishing Co., Singapore, 1999).